Master Thesis

Detectability of dimuon polarization due to ultra-intense magnetic field in non-central Pb-Pb collisions at the LHC ALICE experiment

Graduate School of Science, Hiroshima University
Department of Physical Science,
Experimental Quark Physics Laboratory
M184448

Takumi Osako

February 10, 2020
Supervisor Professor Kenta Shigaki
Chief Examiner Professor kenta Shigaki
Vice Examiner Professor Yasushi Hukazawa

Abstract

In relativistic non-central heavy ion collisions, an ultra-intense magnetic field reaching 1015 [Tesla] can be generated. Many interesting phenomena such as non-linear QED effects and Chiral Magnetic Effects are expected to be induced under the field. Heavy ion collisions are the only experimental way to generate such an intense field and to study the field-induced phenomena.

Di-leptons from virtual photons are a unique tool for probing such an ultra-intense magnetic field because the field-induced birefringence in vacuum enhances dileptons having a specific decay plane with respect to the field. In particular, virtual photons produced in initial collisions can be sensitive to the magnetic field existing at an early stage of the collisions. In this study, we assume the virtual photons from initial collisions as a signal.

The ALICE experiment is dedicated to heavy ion collisions at CERN LHC. Until ALICE Run 2 (until 2018), muons are measured with Muon Spectrometer (MUON). The MUON has high charged particle discrimination by a hadron absorber placed near the collision point. However, due to an absence of a detector before the absorber, multiple scattering makes a muon generation point resolution worse. It is hard to separate muons coming from the collision point from background (BG) muons such as from charged hadrons (CH) and open heavy flavors (HF), whose generation points are away from the collision point. With only MUON, it is found that the detectability of dimuon polarization is lower than 1 σ because of a low signal-to-BG ratio assuming one virtual photon signal having 100% polarization within a detector acceptance in 1000 Pb-Pb events. Therefore, BG rejection at the track level is crucial. From Run 3 (from 2021), the Muon Forward Tracker (MFT) will be newly installed in front of the absorber and it can significantly improve the generation point resolution. Consequently, reduction of the BG level can be achieved.

The simulation study has been made with the polarized virtual photons embedded in the Run 2 data to demonstrate the achievable detectability of dimuon polarization with a variation of BG rejection efficiencies. BG rejection by MFT is implemented manually for muons in the real data with the measured fractions of BG muons from CH and HF in the total muon yield.

Contents

1 Introduction **5**
- 1.1 Standard Model . . . 5
- 1.2 Quark Gluon Plasma (QGP) . . . 5
- 1.3 High Energy Heavy Ion Collision . . . 6
  - 1.3.1 Picture of Collisions . . . 6
  - 1.3.2 Glauber model . . . 8
- 1.4 Magnetic field in heavy ion collisions . . . 8
  - 1.4.1 Principle of the field generation . . . 8
  - 1.4.2 Intensity and Lifetime of the field . . . 9
  - 1.4.3 Field-Induced Phenomena . . . 11
- 1.5 Purpose of this study . . . 12

2 Experimental setup **13**
- 2.1 Large Hadron Collider (LHC) . . . 13
- 2.2 ALICE experiment . . . 13
  - 2.2.1 V0 . . . 14
  - 2.2.2 Muon Spectrometer (MUON) . . . 15
- 2.3 ALICE upgrade . . . 16
  - 2.3.1 Muon Forward Tracker . . . 16

3 Demonstration of Polarization Measurement **18**
- 3.1 Method of Dilepton Polarization Measurement . . . 18
  - 3.1.1 Direct photon production in HIC . . . 18
  - 3.1.2 Definition of polarization in MUON acceptance . . . 20
  - 3.1.3 Kinematic variable to distinguish a relationship between the field and the decay plane . . . 20
- 3.2 How to demonstrate the polarization measurement . . . 23
  - 3.2.1 Virtual photon production in pythia as a signal . . . 24
  - 3.2.2 Run2 real data as a background . . . 25
  - 3.2.3 Detectability of the polarization . . . 25

4 Result and Discussion **26**
- 4.1 Detectability after background subtraction . . . 26
- 4.2 Detectability after low p_{T} cut . . . 27
- 4.3 Detectability assuming background rejection with MFT . . . 29

5 Conclusion **31**

List of Figures

1 QCD phase diagram[1] . . . 6
2 Central and peripheral collision when radius is R[2] . . . 7
3 Pictures before and after collision with an impact parameter b[2] . . . 7
4 N_{coll} and N_{part}[3] . . . 8
5 Magnetic field in HIC[4] . . . 9
6 Intensity of the field soon after the collision by Glauber model[4] . . . 10
7 Large Hadron Collider [10] [11] . . . 13
8 ALICE Detectors[12] . . . 14
9 V0-A and V0-C . . . 15
10 MUON . . . 15
11 MFT . . . 17
12 A and B : Prompt photon production, C and D, Thermal photon production . . . 19
13 Yield of Direct photon [14] . . . 19
14 MUON acceptance . . . 20
15 Reference vector . . . 21
16 θ distribution of not polarized dimuon . . . 22
17 θ distribution of 100% perpendicularly polarized dimuon . . . 22
18 θ distribution of 100% parallel polarized dimuon . . . 23
19 Degree of polarization with three types of dimuon. Black is not, Green is 100% parallel and Red is 100% perpendicularly polarized . . . 23
20 Mass of virtual photon . . . 24
21 Transverse momentum of virtual photon . . . 25
22 θ distribution with 1signal in 1000 Pb-Pb . . . 26
23 P with 1 signal in 1000 Pb-Pb . . . 27
24 θ distribution after low p_{T} cut . . . 27
25 θ distribution after low p_{T} cut . . . 28
26 P after low p_{T} cut . . . 28
27 θ distribution when rejection by MFT is applied . . . 29
28 P when rejection by MFT is applied . . . 30

1 Introduction

1.1 Standard Model

In nature, there are four interactions: gravitational, electromagnetic, strong, and weak interaction. The standard model is the theory that fundamentally describes the hierarchical structure of matter with electromagnetic , strong, and weak interaction. It supports the foundation of basic physics.
The standard model is based on the unified-electroweak theory that unifies the electromagnetic and weak interactions and quantum chromodynamics (QCD) that describes the strong interactions between quarks that constitute matter. In this model, a force is propagated by particles called gauge bosons, and each interaction has a corresponding gauge boson. Gauge bosons corresponding to electromagnetic interaction, strong interaction, and weak interaction are photon, gluon, and weak boson, respectively. Graviton is predicted as a gauge boson corresponding to gravitational interaction, although it has not been discovered yet.

The elementary particles that constitute matter are classified into quarks and leptons, each of which has six types. Quarks have a color charge and an electric charge, and the strong and electromagnetic interaction work. Lepton, on the other hand, has an electric charge but no color charge and is not affected by strong interactions.
Particles composed of quarks are collectively called hadrons. Hadrons are divided into baryon in which three quarks are combined and the total color charge is zero, and mesons in which quarks and anti-quarks are combined. For example, protons and neutrons that constitute the nucleus are hadrons, and pions and kaons are mesons. According to QCD, quarks and gluons interact with each other inside hadrons and cannot be extracted alone. This is called quark confinement. Another feature of QCD is that it has asymptotic freedom, in which the coupling constant of the strong interactions decreases asymptotically in the high energy region.

1.2 Quark Gluon Plasma (QGP)

The keys to release quarks from confinement are the asymptotic freedom and high-temperature, high-density states. Due to the characteristic of asymptotic freedom, the coupling constant of strong interaction decreases with increasing momentum in high-temperature and high-density states. In a high-density state, the gluon has a color charge and causes a self-interaction, thereby weakening the effective intensity of the color charge by a shielding effect. As a result, in a high-temperature and a high-density state, a phase in which quarks and gluons effectively act as free particles is generated. The state in which the quarks and gluons are released from their constraints and their degrees of freedom are revealed is called quark-gluon plasma.
It is thought that a quark-gluon plasma has been realized in the very early universe after the Big Bang and inside neutron stars. Observing QGP is an important clue to study the quark confinement mechanism which is still mysterious, the properties of nuclei and hadrons, and the

early stages of the universe.

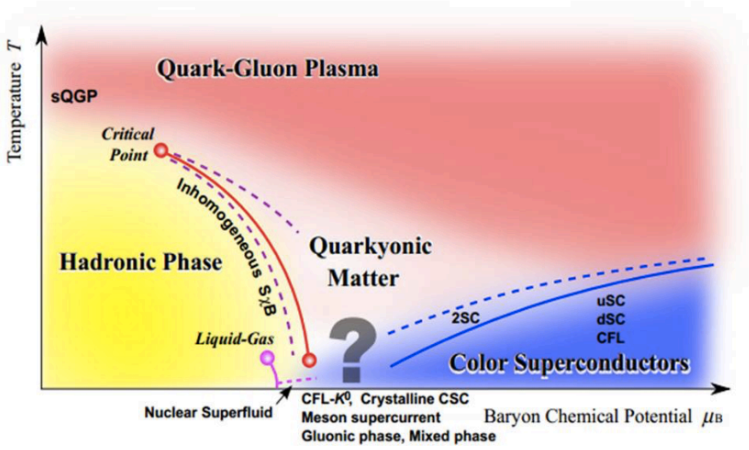

Figure 1: QCD phase diagram[1]

1.3 High Energy Heavy Ion Collision

The high-energy nuclear collision experiment is the only method that can reproduce the high-temperature high-density state on the earth. For research on QGP, heavy ions such as lead or gold are collided with high energy using an accelerator that can accelerate to a relativistic region. Nuclear is the densest substances on earth, and by accelerating them to near the speed of light and colliding them, a huge amount of energy can be packed in a narrow space. In this way, a high-temperature high-density state is artificially created to generate QGP.
Currently, these high-energy nuclear collision experiments are conducted at the RHIC accelerator at the Brookhaven National Laboratory (BNL) in Long Island, New York, USA, and at the LHC accelerator at the European Joint Nuclear Research Organization (CERN) in Geneva, Switzerland. These experiments reproduce the highest temperature that humans can reach in the laboratory, and can be said to be an experiment approaching the elucidation of the early universe. It is hoped that future experiments will elucidate the physical properties of QGP by clarifying and understanding the properties of QGP, and further clarify the properties of matter in the early universe and in the extremes of high temperatures.

Here the picture of high energy nuclear collision is shown.

1.3.1 Picture of Collisions

The nuclear collision is classified by impact parameter b [fm]. The impact parameter is defined by the distance between centers with respect to the direction of nucleus propagation. If b$\sim$0, it is called a central collision, and if b $<$ 2R, it is called a non-central, mid-central or peripheral

collision. The radius of nuclear differs between various nucleus, so centrality is more often used rather than impact parameter. Centrality is defined as 0% to 100% for 0 to 2R of impact parameter.

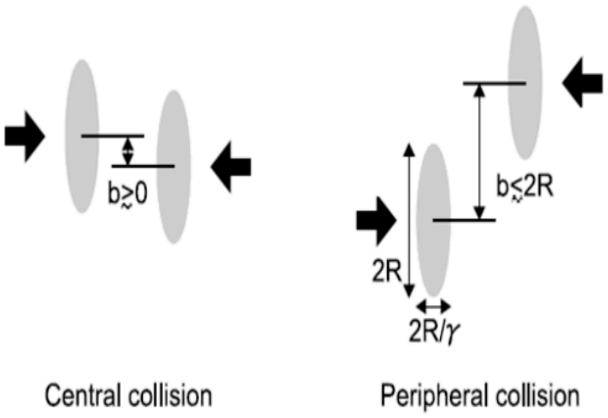

Figure 2: Central and peripheral collision when radius is R[2]

In the case of central collision, all nucleons participate in the collision when the same nuclei are collided, whereas in the case of non-center collision, only the overlapping parts are involved in the collision. The part involved in the reaction is called a "participant", and the part that passes without being involved in the reaction is called a "spectator". The spectator flies near the speed of light, but the participant changes depending on the collision energy. Fig. 4 shows a state before and after a nuclear collision with an impact parameter b.

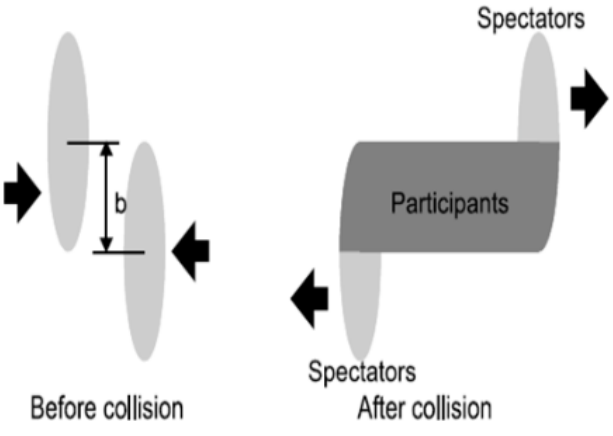

Figure 3: Pictures before and after collision with an impact parameter b[2]

1.3.2 Glauber model

The Glauber model describes the geometric picture of high energy nuclear collisions accurately. Considering a nuclear collision as a superposition of nucleon-nucleon collisions, and assuming that trajectories of nucleons do not change even after collision.
In the Glauber model, the number of nucleon-nucleon collisions (N_{coll}) and the number of participants (N_{part}) can be obtained as a function of b by giving the initial distribution of colliding nuclei and the nucleon-nucleon interaction cross section. It is impossible to determine b in an actual experiment, so the experimental data are compared with the Glauber model to determine the centrality. FIG. 5 shows the b dependence of N_{coll} and N_{part} calculated by Monte Carlo simulation.

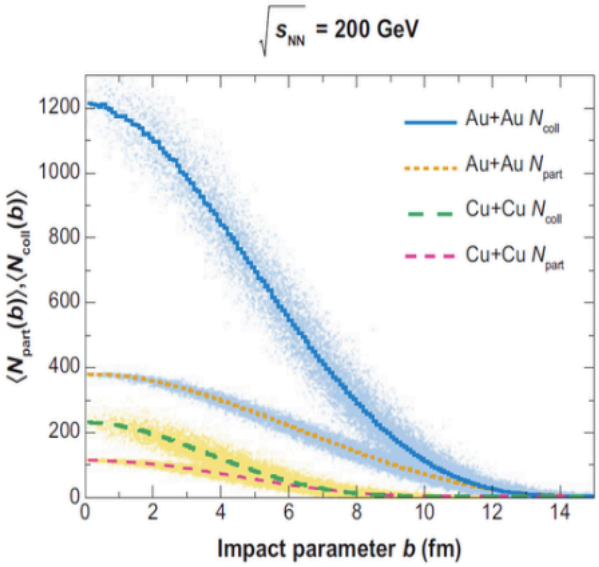

Figure 4: N_{coll} and N_{part}[3]

1.4 Magnetic field in heavy ion collisions

1.4.1 Principle of the field generation

The possibility of generating strong magnetic fields in high-energy nuclear collisions was predicted about 30 years ago. Its maximum intensity reaches 10^{15} Tesla in the LHC accelerator energy region of CERN, which is the highest intensity of any magnetic field existing in the universe. Although special phenomena under strong fields have been discussed from a theoretical perspective, they have not been verified under magnetic fields exceeding the critical magnetic field. Therefore, in recent years, the presence of a strong magnetic field in high-energy nuclear

collision has attracted an attention.
The principle of a magnetic field generation in high energy nuclear collisions can be explained by classical electromagnetic dynamics. In high energy nuclear collisions, large charged nuclei (In LHC, Pb : Z = 82 is mainly used) are accelerated and collided to near the speed of light. When a charged particle moves, a magnetic field is generated. When nuclei collide with each other at the center, the generated magnetic field is generated symmetrically with respect to the collision point. They cancel each other out and become zero. However, in a non-central collision in which nuclei collide with each other with a finite distance, a very intense magnetic field is generated around the collision origin because of the spectator. FIG. 7 shows a state of the field generation in high energy nuclear collision. As shown in the figure, the field is generated perpendicular to the plane formed by the beam axis (z axis) and axis connecting the centers of the nuclei (x axis) and this is called a reaction plane. Furthermore, these occur on a spatial scale as narrow as 10 fm. Since the generated field is inversely proportional to the distance, the field is intense.

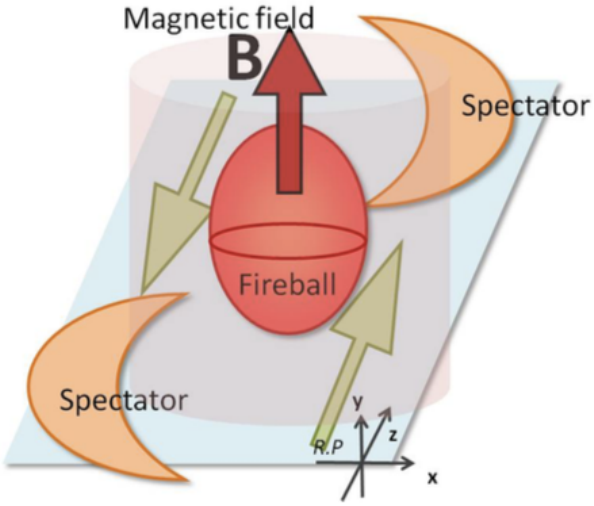

Figure 5: Magnetic field in HIC[4]

1.4.2 Intensity and Lifetime of the field

Since nuclei accelerated to near the speed of light collide, relativistic effects must be taken into account when calculating the strength of the strong magnetic field. The magnetic field created by a relativistic charged particle at time t and position $\boldsymbol{r}$ is described by the Lienard-Wiechert potential equation (1.1).

$$\boldsymbol{B}(\boldsymbol{r},t) = \frac{e\mu_0}{4\pi}\frac{\boldsymbol{\nu}\times\boldsymbol{R}}{R^3}\frac{(1-v^2/c^2)}{[1-(v/c)^2 sin^2\phi_{R_\nu}]} \tag{1}$$

Where $\boldsymbol{R}$ = $\boldsymbol{r}$-$\boldsymbol{r}'$, μ_0 is the magnetic permeability of the vacuum, ϕ_{R_ν} Is the angle between $\boldsymbol{R}$ and $\boldsymbol{\nu}$. If we can know the position and velocity of each charged particle, we can find the strength of the magnetic field generated by each particle, and by adding it up to all charged particles, we can find the strength of the field generated by nuclear collisions . According to this calculation, the maximum intensity of the field reaches about 10^{15} Tesla. The maximum stable magnetic field that can be generated in the laboratory is about 1000 Tesla, but a high-energy nuclear collision can generate a magnetic field as large as 12 orders of magnitude.

FIG. 8 shows the dependence of the intensity of the magnetic field generated by the incident protons involved in the collision at t = 0 immediately after the collision using the Glauber model on the collision coefficient by Monte Carlo simulation.

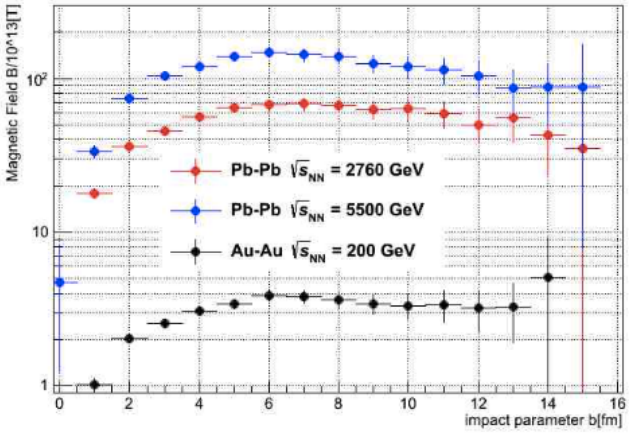

Figure 6: Intensity of the field soon after the collision by Glauber model[4]

In all energies, the magnetic field is relatively weak in the central collision, and the intensity increases as the impact parameter increases. The intensity reaches its maximum at b = 6 $\sim$ 10 fm. This corresponds to 30 $\sim$ 60% in terms of centrality. Then, as for a central collision, the magnetic field weakens due to the decrease of N_{coll}. The intensity is proportional to the collision energy, and the maximum intensity of the magnetic field reaches 10^{14} Tesla in the RHIC energy region and 10^{15} Tesla in the LHC energy region.
As explained in 1.3.1, at the time of collision, particles are divided into participant and spectator. Since the spectator flies off at the speed of light after the collision, it generates an extremely strong magnetic field in the direction perpendicular to the reaction plane, but it fluctuates quickly as it flies away. FIG. 9 shows the time dependence of the strong magnetic

field calculated by the hadron cascade model. From this, the magnetic field has decreased by one digit after 0.1 fm / c and by four orders of magnitude after 1 fm / c, and it has been previously discussed how much the effect of this magnetic field can be realized.However, in recent years, the existence of the effect of extending the life of the magnetic field due to the conductivity of QGP and the possibility of the magnetic field due to the rotation of QGP have been discussed, and these have reduced the effect of the magnetic field. It is said that it will be so large that it cannot be ignored. In addition, since electromagnetic probes such as photons and electrons generated immediately after collision are not affected by strong interaction, they are expected to be detected with the influence of strong magnetic fields. Observing this effect is expected to provide evidence that a high magnetic field is generated by high energy nuclear collisions.

1.4.3 Field-Induced Phenomena

It is very interesting to see how the field affects the dynamics of high energy nuclear collisions. Here, phenomena associated with generation of a strong magnetic field are briefly described.

Synchrotron radiation of quarks[6]

There are many quarks and gluons released from confinement in the QGP phase. When a strong magnetic field is generated there, the quarks have electric charges, and emit a gluon around the magnetic field. This is the same phenomenon that an electron wraps around a magnetic field and emits photons. This phenomenon occurs because the binding constant of QCD is sufficiently larger than that of QED. When a quark or antiquark emits gluon, the quark or antiquark causes energy loss. Normally, it is considered that energy loss is caused by passing through a high-temperature substance, so that energy loss due to synchrotron radiation is regarded as a new cause of energy loss. In [6], energy loss per length is obtained as a function of lateral momentum.

Photon splitting[7]

Furry's theorem prohibits such processes with an odd number of outer lines; however, this three-point interaction is possible in a magnetic field. It can happen that a real photon splits into two photons, a phenomenon that can also occur in high-energy nuclear collisions, where the splitting of a photon can change the photon's energy distribution in a softer way.

Chiral Magnetic Effects[8]

Although this is not the effect of nonlinear QED, it is an interesting phenomenon that shows the relationship between QED and QCD.
The chiral magnetic effect is a phenomenon in which a current flows in a direction parallel to a magnetic field due to a topological transition in a strong magnetic field. It is impossible to

observe the current itself in actual high-energy collision experiments, but it is thought that fluctuations in charge symmetry caused by the current are evidence of the chiral magnetic effect. The RHIC STAR experimental group observes fluctuations in charge symmetry that cannot be explained by theoretical calculations without incorporating topological effects. [9]
There are also very interesting discussions, such as the possibility that experimental verification of the chiral magnetic effect may be evidence of restoration of chiral symmetry, and the possibility of CP violation associated with the chiral magnetic effect.

CME is currently being studied energetically because it is considered to be a very interesting physics and a signal of a magnetic field, but no definitive results have yet been obtained. Furthermore, it is controversial whether this charge separation is really caused only by CME, in other words, whether CME is a suitable signal for magnetic field detection.

Birefringence in vacuum[5]

Therefore, detection of a magnetic field by vacuum birefringence has been proposed in the past[5]. This is one of the effects of nonlinear QED. Nonlinear QED is a phenomenon caused by perturbation expansion breaking when an external field stronger than the critical magnetic field of electrons is given. The critical magnetic field is about 10^{10} Tesla, and the magnetic field generated by nuclear collisions can be expected to cause this phenomenon sufficiently. Vacuum birefringence means that a magnetic field breaks Lorentz symmetry, causing photons to respond differently depending on their momentum direction. For example, considering a virtual photon that decays into a lepton pair (a photon that has a mass for a very short time due to the uncertainty principle), if the momentum is parallel to the magnetic field, the decay plane of the decaying lepton pair is isotropic with respect to the magnetic field. It is a target. However, if the momentum is perpendicular to the magnetic field, the decay plane of the lepton pair may be anisotropic with respect to the magnetic field. In this study, this anisotropy is defined as "Polarization", and observing this polarization enables magnetic field detection.

1.5 Purpose of this study

We aim at direct detection of strong magnetic field generation in high energy nuclear collisions. In the past, the possibility of detection using an electron pair as a probe was discussed in experimental data of 2.76 TeV lead-lead collision per LHC nucleon [4] [5]. Not in. In this study, we discuss the possibility of detecting a strong magnetic field based on LHC experimental data for the detection of a strong magnetic field using a muon pair as a probe, which we plan to perform in the future.

2 Experimental setup

2.1 Large Hadron Collider (LHC)

The LHC accelerator is the world's largest circular hadron collider built by the European Union Atomic Energy Agency (CERN) on the outskirts of Geneva, Switzerland. It is built approximately 100 m underground across the French-Swiss border near CERN and has a circumference of 26.7 km. In the LHC accelerator, it is planned that the proton-proton collision will achieve a center-of-gravity collision energy of 14 TeV, and the lead-lead collision will achieve a center-of-gravity collision energy of 5.5 TeV per nucleon pair.
The purpose of the LHC accelerator is to discover Higgs and supersymmetric particles in proton-proton collision experiments and to clarify the properties of QGP in lead-lead collision experiments. The LHC accelerator has six experimental groups: ALICE, ATLAS, CMS, LHC-b, TOTEM, and LHC-f. Each experimental group targets different physics. For example, in ATLAS experiments and CMS experiments, we focus on high-energy proton-proton collisions at the LHC and analyze the particles generated by the collisions to discover Higgs particles that contribute to the mass of matter and to exceed the standard model. Aiming at exploration of new physics.

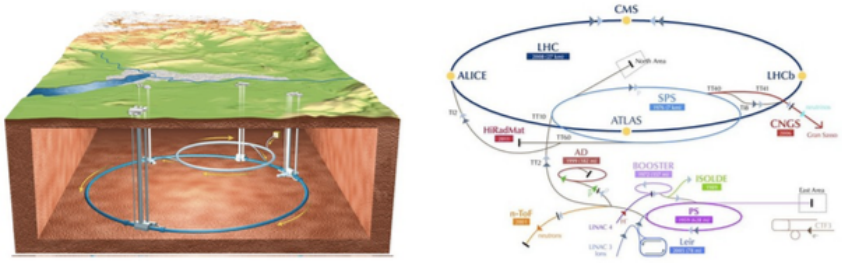

Figure 7: Large Hadron Collider [10] [11]

2.2 ALICE experiment

The ALICE (A Large Ion Colider Experiment) experiment is one of six experiments to be performed at the LHC accelerator. Nuclear collisions at the LHC accelerator produce temperatures more than 100,000 times that of the central sun. The quark in the nucleon is released from confinement, and a QGP phase, which is thought to have existed in the very hot universe immediately after the Big Bang, appears. If the QGP phase is observed by the ALICE experiment, it may be a clue to how the materials that make up the current universe were generated through the expansion and cooling of the universe from the Big Bang, and how they were generated.
The ALICE experiment is the only experiment dedicated to heavy ion collision experiments and focuses on the elucidation of QGP, so it is designed to measure many physics. When

nuclei accelerated by the LHC collide with each other, thousands of various particles are generated.For QGP phase observation, the large number of generated particles are distinguished, and the momentum and energy are precisely measured. There must be. As a detector, of course, high detection efficiency and high energy and position resolution are required. The ALICE detector is capable of recognizing the tracks of particles in a wide range of momentum, and is also capable of handling the maximum particle multiplicity of lead-lead nuclear collisions at LHC energies. It consists of a large number of detectors, and is a huge detector with a height of 16 m, width of 16 m and depth of 26 m.Figure 11 shows the entire detector of the ALICE experiment.

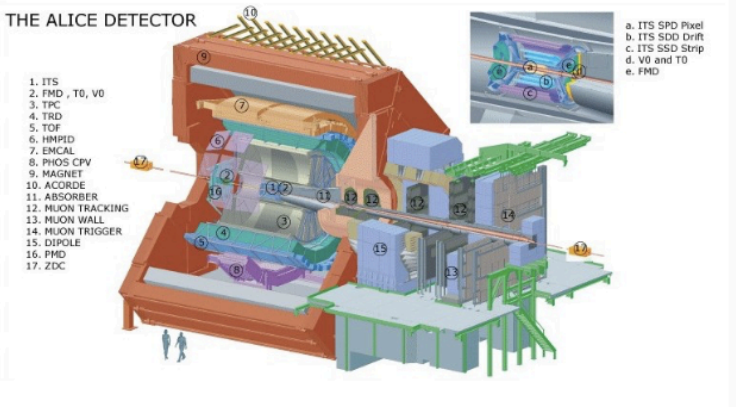

Figure 8: ALICE Detectors[12]

In this study, we mainly use data obtained from the following detectors.

2.2.1 V0

V0 is composed of two scintillators (V0-A, V0-C). These are front particle detectors installed at z = -90 cm and +340 cm, respectively, covering $2.8 < \eta < 5.1$ and $-3.7 < \eta < -1.7$. A schematic diagram is shown in Figure 13 below. The V0 detector is a trigger detector and can distinguish between background events such as beam gas events and collision events. In addition, the luminosity, charged particle multiplicity, collision centrality, and event plane of nucleus collisions are measured. When nuclei collide, if there is a central collision event with the largest number of generated particles such that the nuclei collide head-on, there will also be a peripheral collision event where the nuclei collide. Since the physics that can be verified from each event is different, this detector is used to perform measurements separately.

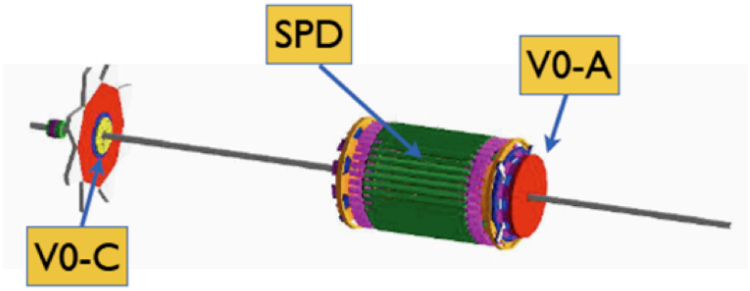

Figure 9: V0-A and V0-C

2.2.2 Muon Spectrometer (MUON)

Reconstruct muon tracks using a 5-layer pad chamber in the range of -4.0 $< \eta <$-2.5. A magnetic field of 0.7 Tesla is applied to this area, and the momentum is measured. Muon is identified using a two-layer cathode pad chamber behind it. In the muon detection using a muon spectrometer, in order to utilize the high muon penetration power, absorbers with large mass numbers are installed at two locations, and the transmitted particles are identified as muons. The first absorber is composed of 4m ($\sim$ 10 λ) of carbon, and is installed in the rapidity direction where the muon spectrometer is located. Here, only muons with momentum $p = 4$ GeV/c ($p_{\mathrm{T}} \geq$ 0.5 GeV/c) or more can pass. The second absorber is a 1.2m ($\sim$ 7 λ) thin absorber made of iron, and is installed between the five-layer and two-layer chambers behind it. This absorber removes hadron-derived secondary particles that appeared in the front absorber [12].

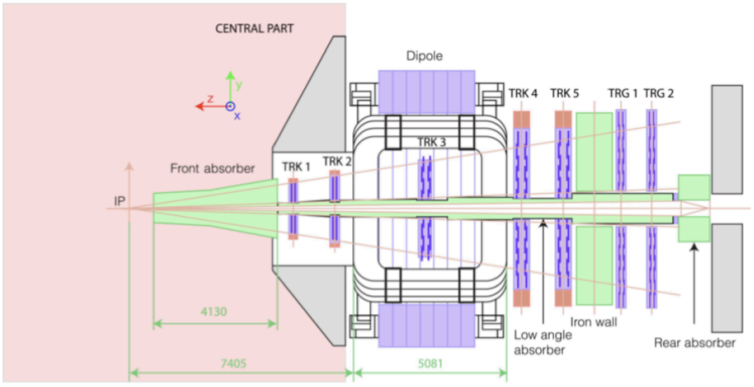

Figure 10: MUON

2.3 ALICE upgrade

The detector will be improved and a new detector will be introduced for Run3, the next advanced plan, which will start in 2021. The ALICE experiment aims to increase the amount of data acquired from Run3 and improve track reconstruction accuracy. The goal is to accumulate an integrated luminosity of 10 nb^{-1} of muon trigger in the forward direction of the Pb-Pb collision, which is about 45 times that of the current experiment Run2. This section describes the forward silicon pixel detector MFT to be introduced.

2.3.1 Muon Forward Tracker

Muon-forward tracker (MFT) is a silicon pixel detector installed between the collision point and the front absorber to improve the track reconstruction accuracy near the collision point. The already installed muon spectrometer is designed to improve the track reconstruction accuracy near the collision point, and more accurate measurement of QGP characteristics in the forward region is expected. It is installed along the beam axis and covers a pseudorapidity of -3.6 $<$ η $<$-2.45 in the range of 460 $<$ z $<$ 768 mm. Figure 16 below shows a schematic diagram of the entire MFT. MFT improves the generation point resolution by measuring muons before undergoing multiple scattering at the absorber. As a result, it becomes possible to remove charged hadron-derived muons and to separate heavy quarks, which could not be achieved by existing detectors alone.

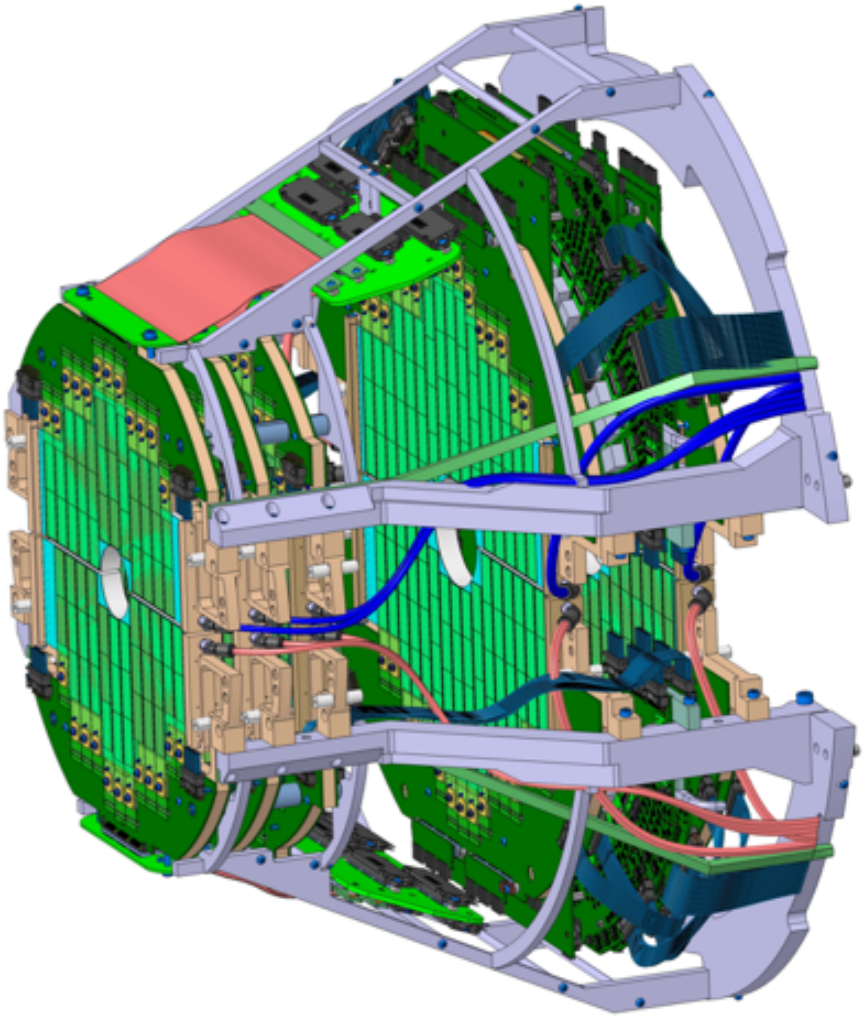

Figure 11: MFT

3 Demonstration of Polarization Measurement

3.1 Method of Dilepton Polarization Measurement

In this section, a method of the polarization measurement and a demonstration of experimental measurement are described.

3.1.1 Direct photon production in HIC

As described above, in order to induce muon pair deflection by a magnetic field, the magnetic field and the photons must be in the same space. Since the magnetic field reaches its maximum immediately after the collision and decays shortly thereafter, photons also need to be generated early in the collision. Such photon is called a prompt photon and is produced only by the hard parton scattering early in the collision. In this study, this prompt photon is considered as a signal.
Many photons (γ) are also generated during high energy nuclear collisions. The majority of photons are hadron decay photons from $\pi^0 \to 2\gamma$. However, some photons are directly generated from collisional reactions. Of the photons generated in various processes, components excluding photons caused by the hadron decay process are called direct photons. Direct photons include the contribution of initial parton collisions and parton bremsstrahlung, and the contribution of thermal radiation from the impinging system. The former mainly consists of quark and gluon QCD Compton scattering, quark / antiquark annihilation, quark bremsstrahlung, etc., and is a good reference measurement of the initial parton distribution. The latter is expected as a direct signal of parton thermal equilibrium. The strength of the interaction between photons and quarks is as small as the fine structure constant $\alpha \sim 1/137$, and photons do not interact directly with gluons. Thus, photons pass through with little interaction with the material created in the reaction zone and are measured.
Since hadron decay photons are secondary photons created after the end of a nuclear collision reaction, they do not directly hold information at the beginning of the reaction or in the reaction region. On the other hand, since direct photons are produced in the reaction region, the initial stage of the reaction and information in the reaction region can be known. Measuring direct photons is very important, and hadron decay photons are the background for that measurement. There are the following three types of direct photons.

1. Perturbative QCD direct photons from scattering between quark and gluon

2. QGP thermal photons generated from high-temperature QGP

3. Hadron gas thermal photons generated in hadron gas

The direct photons measured experimentally are the sum of those described above, but the magnitude of the lateral momentum differs depending on the generation mechanism. In the high transverse momentum region, perturbed QCD direct photons are the dominant component of direct photons. On the other hand, in the low lateral momentum region, the thermal photons from QGP are expected to be the dominant components of direct photons.
Fig. 13 shows the yield distribution of direct photons in 2.76 TeV lead-lead collisions per nucleon pair. The red line is the region where thermal photons are dominant and can be fitted with a Boltzmann distribution. The blue line is the result of NLO (Next Leading Order) pQCD calculation. According to NLO calculations, thermal photons are dominant when the transverse momentum is less than 3-5 GeV, and perturbative QCD direct photons dominate above that.

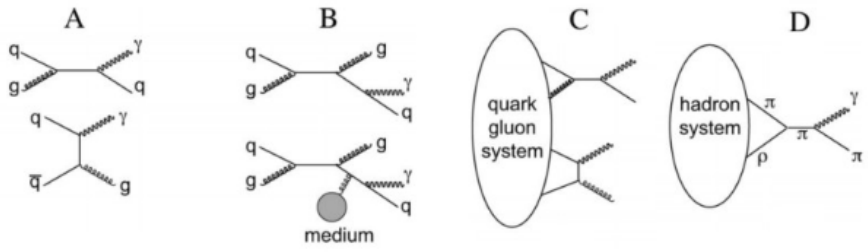

Figure 12: A and B : Prompt photon production, C and D, Thermal photon production

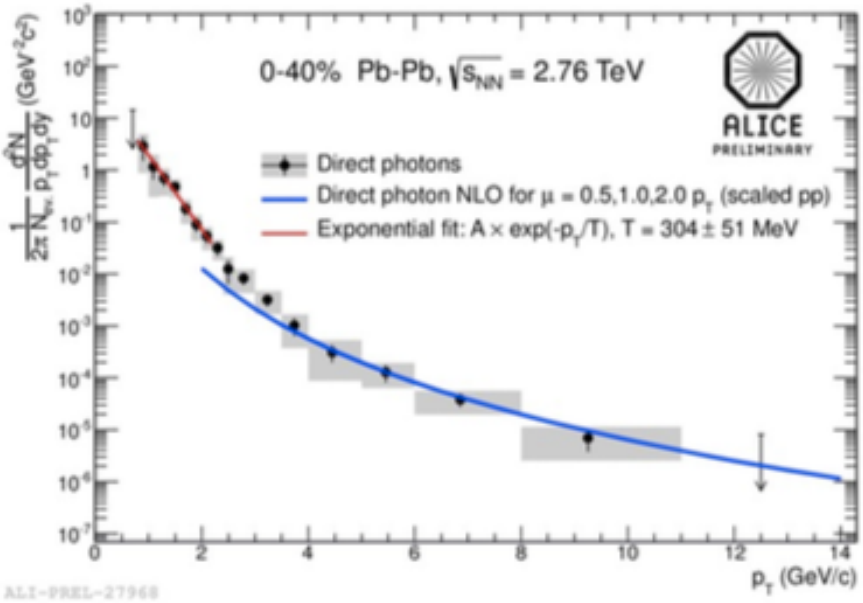

Figure 13: Yield of Direct photon [14]

3.1.2 Definition of polarization in MUON acceptance

Virtual photons are affected by a magnetic field[5] if they have momentum perpendicular to the magnetic field. Considering the MUON detection range, it can be seen that the virtual photons that enter the range always have momentum perpendicular to the magnetic field. The order of dimuon polarization is quantitively estimated[20] and O(10^{-1}) of polarization is expected.

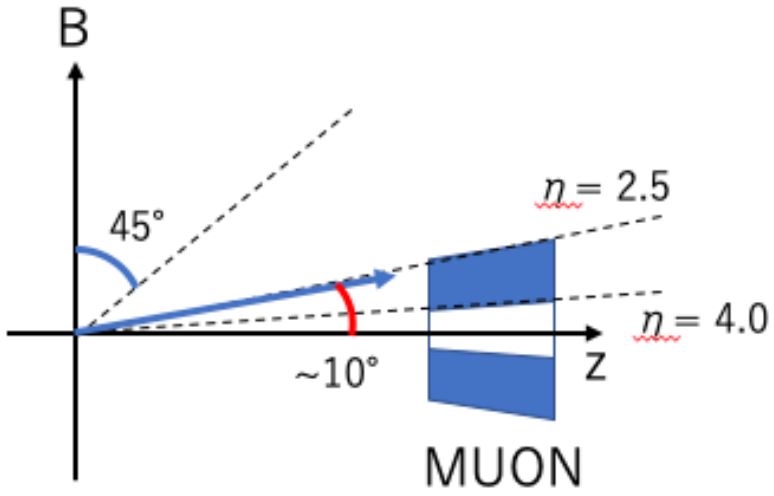

Figure 14: MUON acceptance

From here, the degree of deflection P is defined as

$$P \equiv \frac{N_{\parallel} - N_{\perp}}{N_{\parallel} + N_{\perp}} \tag{2}$$

Here, $N_{\perp}$、$N_{\parallel}$ mean the number of dimuons whose decay planes are perpendicular and parallel to the magnetic field, respectively.

3.1.3 Kinematic variable to distinguish a relationship between the field and the decay plane

Following quantity is used to calculate $N_{\perp}$、$N_{\parallel}$.

$$\theta = \cos^{-1}\left(\frac{\vec{n}_{\mu\mu} \cdot \vec{n}_{\mathrm{ref}}}{|\vec{n}_{\mu\mu}|\,|\vec{n}_{\mathrm{ref}}|}\right) \tag{3}$$

Here, $\vec{n}_{\mu\mu}$ is the cross product of the momentum vector of the muon pair, and $\vec{n}_{\mathrm{ref}}$ is the following vector.

$$\vec{n}_{\mathrm{ref}} = \left(\vec{P}_{\mu^+} + \vec{P}_{\mu^-}\right) \times \left(\vec{P}_{\mu^+} + \vec{P}_{\mu^-}\right)_{\mathrm{RP}} \tag{4}$$

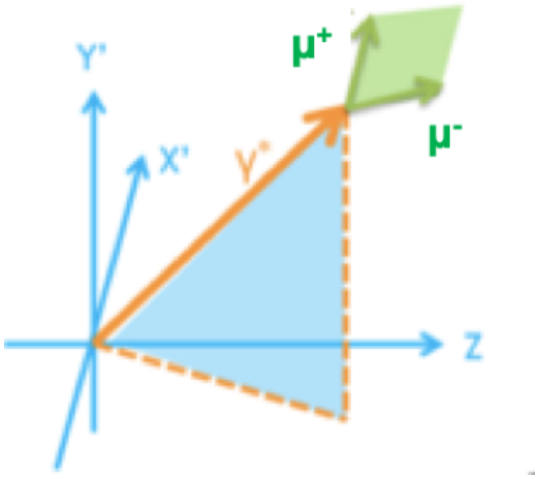

Figure 15: Reference vector

θ represents the angle between the decay plane and the reference plane. Since the reference plane contains information on the magnetic field, the relationship between the decay plane and the magnetic field can be expressed. The number of muon pairs in the vertical and parallel directions is calculated by integrating the angle distribution obtained by this variable in each region.

The behavior of this reference vector with respect to muon pairs that are not deflected, completely vertically deflected, and completely parallel deflected was determined by Monte Carlo simulation. The following is the angular distribution.

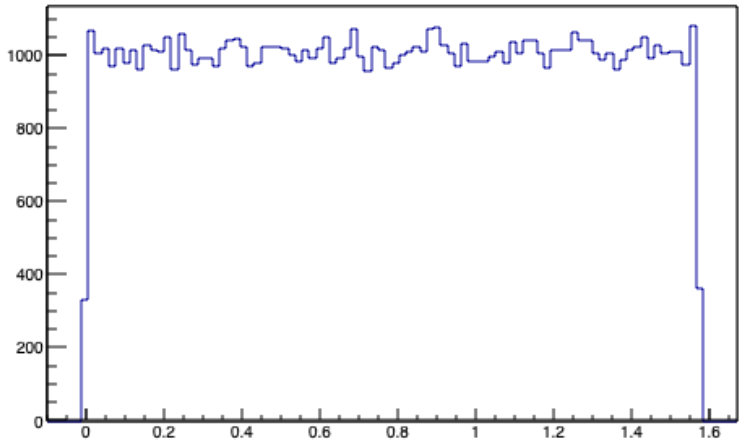

Figure 16: θ distribution of not polarized dimuon

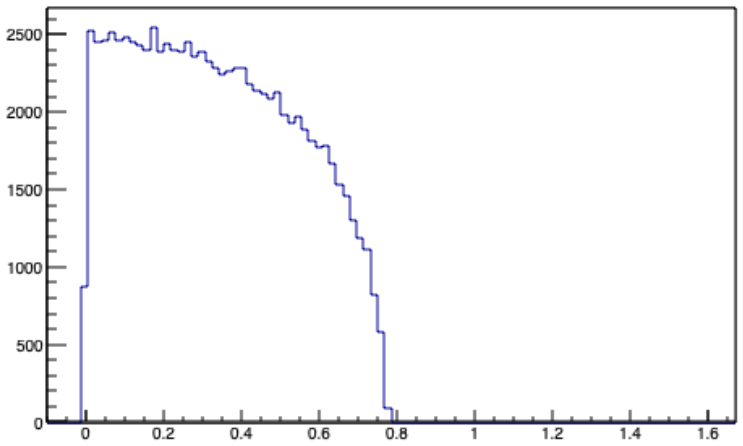

Figure 17: θ distribution of 100% perpendicularly polarized dimuon

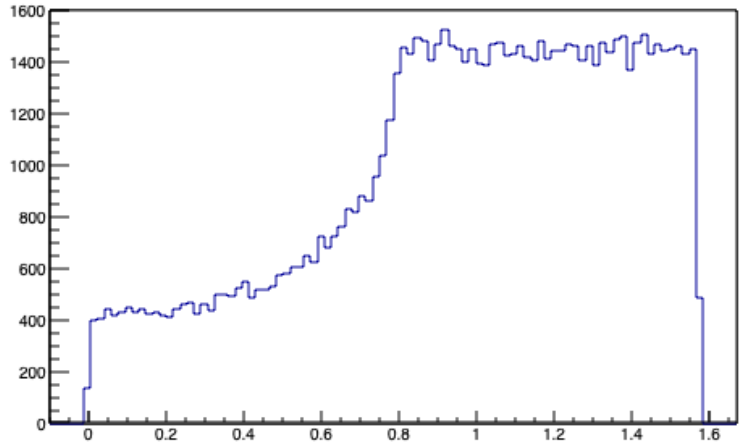

Figure 18: θ distribution of 100% parallel polarized dimuon

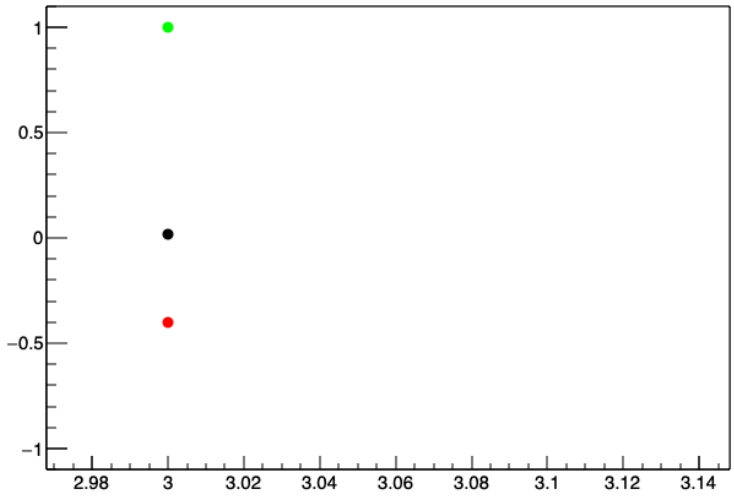

Figure 19: Degree of polarization with three types of dimuon. Black is not, Green is 100% parallel and Red is 100% perpendicularly polarized

By using this reference vector, the value of P becomes 0 for a dimuon that is not deflected, and becomes a positive or negative value for a dimuon that is completely polarized in parallel and perpendicularly. Thereby, the degree of polarization can be quantitatively evaluated.

3.2 How to demonstrate the polarization measurement

This section describes a simulation method assuming actual deflection measurement. Originally, when such a simulation is performed, data obtained by reproducing experimental data

using Monte Carlo simulation is often used as a background, instead of data obtained in an experiment. This is because it is possible to know the particle information that cannot be obtained from the experimental data, and it is useful for understanding the background in detail. There are event generators that generate high-energy nuclear collision events, but they do not reproduce all of the actual experimental data, and some effects (such as fluid effects) do not take into account. In this study, such effects cannot be ignored, so we use actual experimental data as background events, generate them by Monte Carlo simulation, and create data by adding signals with arbitrarily adjusted parameters.

3.2.1 Virtual photon production in pythia as a signal

The signals are dimuons derived from virtual photons created using an event generator called pythia[21]. Virtual photon-derived dimuon are generated by Monte Carlo simulation based on the lateral momentum, mass, and generation probability of virtual photons obtained by pythia. Since pythia is a proton-proton collision simulator, it needs to be scaled to a lead-lead collisions to mix with the background. Since we assume the photons generated by the initial nucleon collisions, we scale into the lead-lead collisions using N_{coll}, which represents the number of nucleon-pair collisions. As a result of the scaling, it was found that there is one virtual photon-derived muon pair in the MUON acceptance at approximately 1000 Pb-Pb in 40% - 60% centrality. The transverse momentum and mass distribution of virtual photons are shown below.

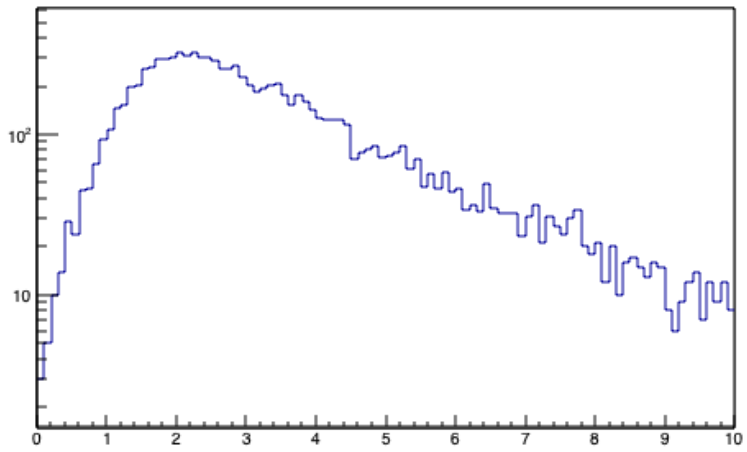

Figure 20: Mass of virtual photon

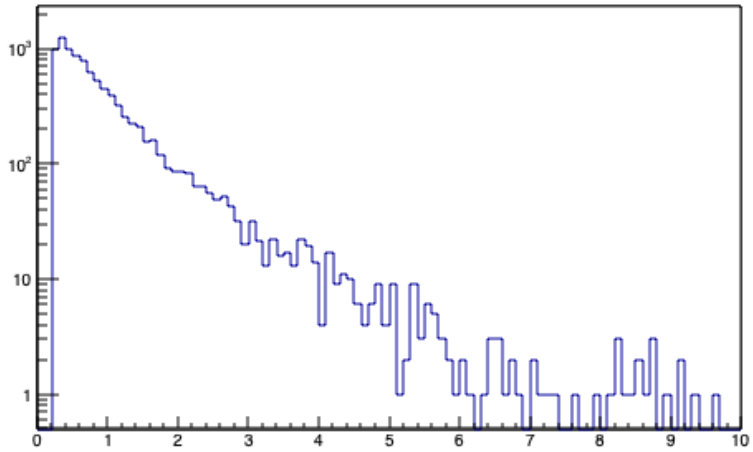

Figure 21: Transverse momentum of virtual photon

3.2.2 Run2 real data as a background

As background, the actual data of Run2 ($\sim$ 2018), whose collision energy is closest to Run 3 planned from 2021 to 2024 at present, was used. Below is a comparison between the data of Run2 and Run3.

	Run 2 real data	Run 3 expected
Energy	5.02 TeV	5.5 TeV
Statistics	4.4×10^8	6.5×10^{10}

Centrality is 40% - 60% considering the intensity of the magnetic field (See 1.4.2) and N_{coll} because prompt photon is linearly increase with N_{coll}.

3.2.3 Detectability of the polarization

The detectability of polarization is determined by the significance of the polarization. The error in the degree of polarization is

$$\pm\sqrt{\text{Var}(P)} = \pm\frac{2}{N_{\parallel}+N_{\perp}}\sqrt{\frac{N_{\parallel}N_{\perp}}{N_{\parallel}+N_{\perp}}} \tag{5}$$

And the ratio between the degree of polarization and the error is the detectability. The error after subtraction of uncorrelated dimuon was obtained using error propagation.

In addition, to improve the detectability, I also evaluate the detectability under the assumption of the removal efficiency of charged hadrons and muons derived from heavy quarks by cutting the transverse momentum region and MFT.

4 Result and Discussion

4.1 Detectability after background subtraction

This shows the angle distribution of dimuons created from a data set with one signal in 1000 Pb-Pb, which is estimated in 3.2.1.

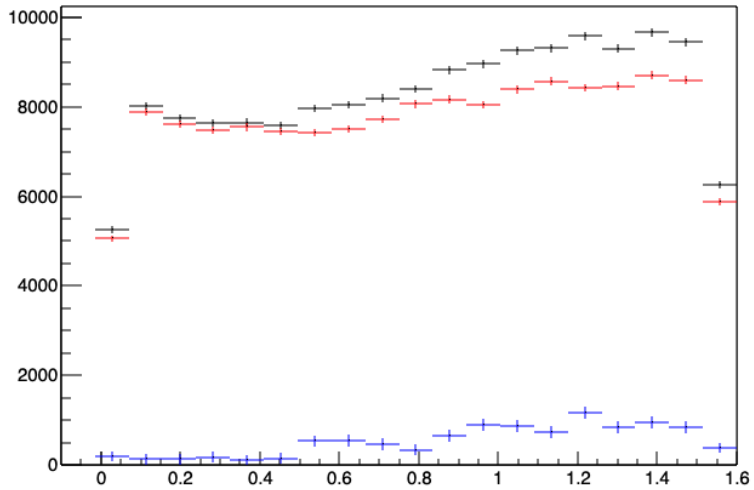

Figure 22: θ distribution with 1signal in 1000 Pb-Pb

The black line is all dimuons, the red line is uncorrelated dimuons reproduced by event mixing which is background, and the blue line is black minus red which means correlated dimuons, such as vector mesons, open heavy flavors and signals. A finite Polarization is found in all dimuons, but as you can see also a finite polarization in uncorrelated dimuons, this means background creates a false polarization. This has to be subtracted as it makes the degree of polarization appear large. And the degree of polarization was 0.8 σ assuming a 10% polarization. (See 3.1.2 and 3.2.3)

all p_{T}	$N_{\perp}$	$N_{\parallel}$
All dimuon	97449	100891
Uncorrelated	92509	92613.8

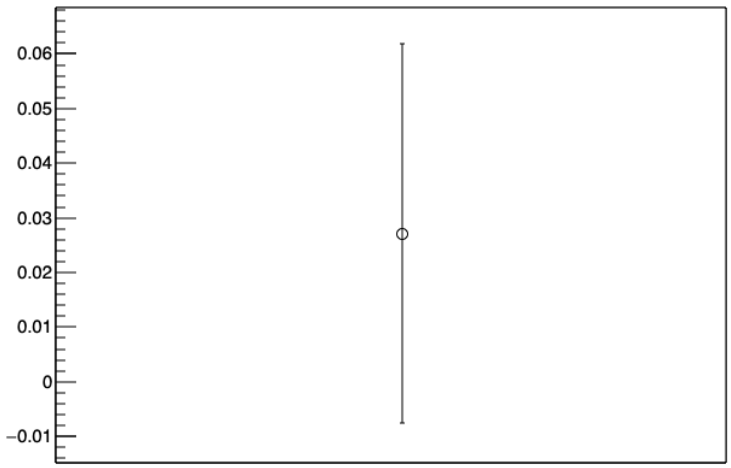

Figure 23: P with 1 signal in 1000 Pb-Pb

4.2 Detectability after low p_{T} cut

The virtual photons, which are signals, are dominant as for direct photons in the high transverse momentum ($>$ 4 GeV/c) region. Since uncorrelated dimuons are mainly distributed in low transverse momentum region, the detection sensitivity can be improved by appropriately cutting them.The following is a comparison between the angular distribution when the high transverse momentum region is selected and the angular distribution in the entire region. Following table shows $N_{\perp}$ and $N_{\parallel}$.

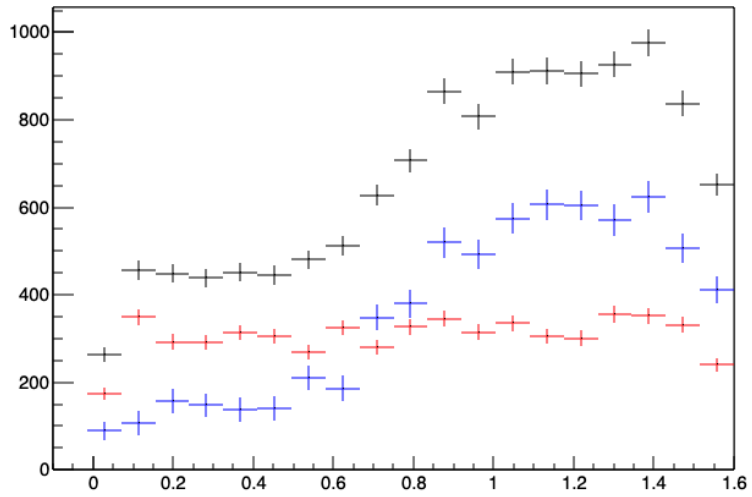

Figure 24: θ distribution after low p_{T} cut

all p_T	$N_\perp$	$N_\parallel$
All dimuon	97449	100891
Uncorrelated	92509	92613.8

low p_T cut	$N_\perp$	$N_\parallel$
All dimuon	5860	7911
Uncorrelated	3707	3858

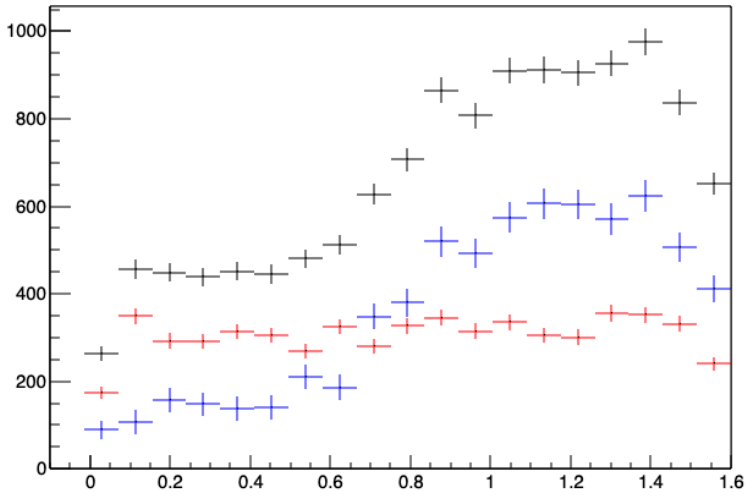

Figure 25: θ distribution after low p_T cut

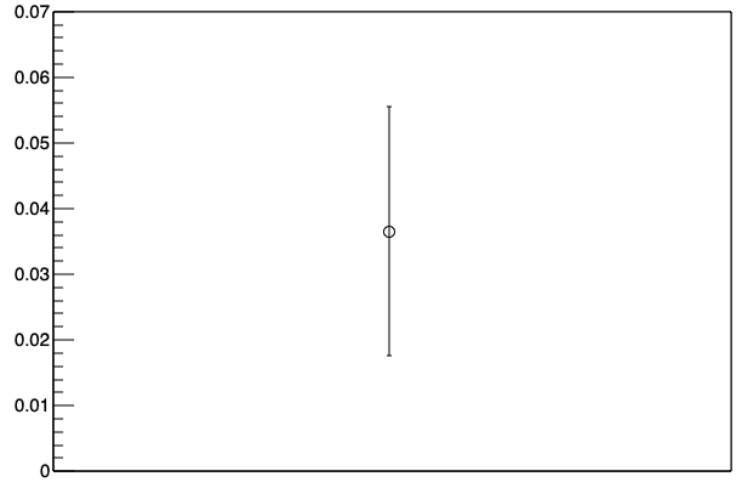

Figure 26: P after low p_T cut

The detection sensitivity increases 0.8 σ to 1.9 σ by cutting low p_{T} region.

4.3 Detectability assuming background rejection with MFT

As described in 2.3.1, introduction of MFT can remove the main background muons from charged hadrons and from heavy quarks. The respective removal efficiencies are currently being evaluated. Here, the detection sensitivity assuming a certain removal efficiency is calculated, and the maximum sensitivity in Run 3 is evaluated.The following is the angular distribution when the heavy quark-derived muon removal efficiency is 30 % and the charged hadron-derived muon pair removal efficiency is 50%[23].

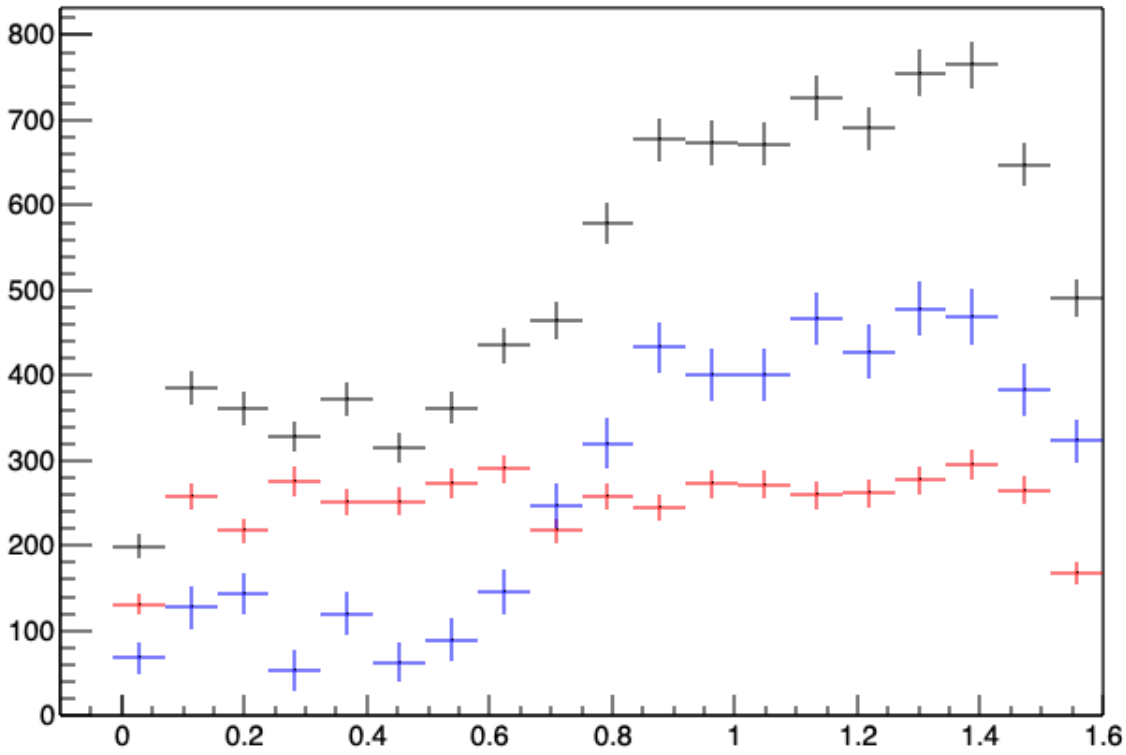

Figure 27: θ distribution when rejection by MFT is applied

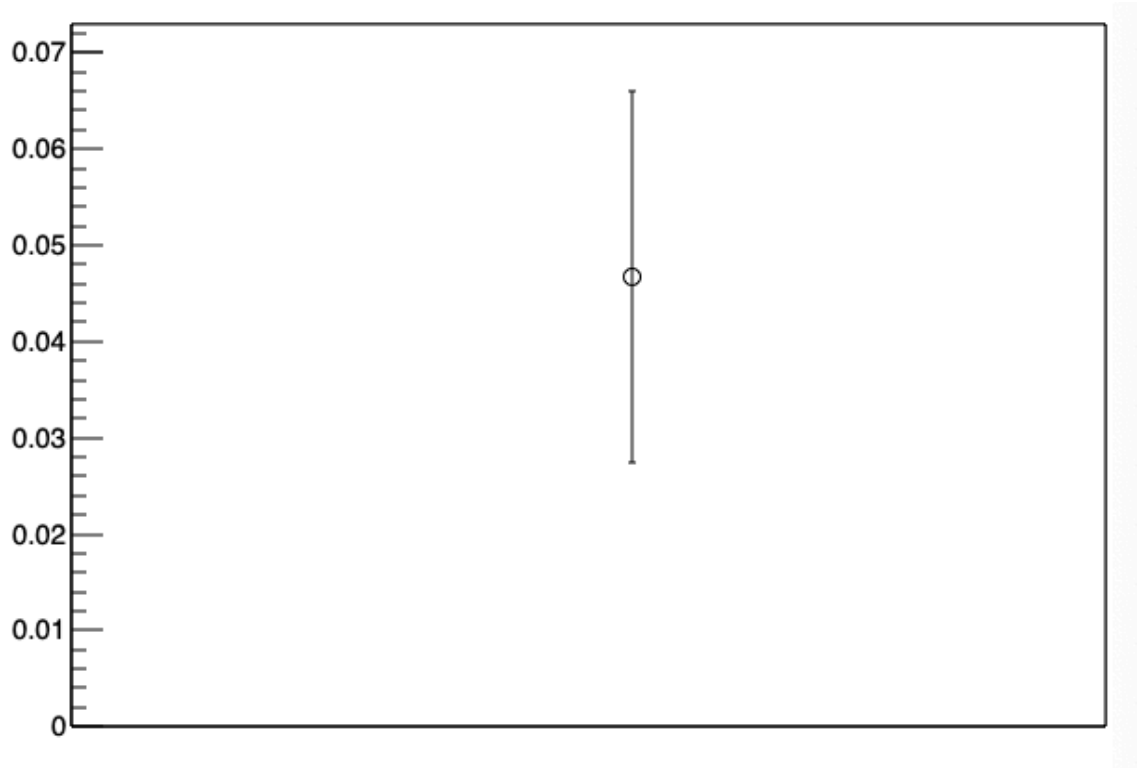

Figure 28: P when rejection by MFT is applied

It was found that the detection sensitivity reached 2.5 σ when the efficiency of removing hadrons derived from charged hadrons was 50%. Furthermore, considering the statistics in Run 3, this detectability becomes ten times better(See 3.2.2). This suggests that there is great promise for future detection.

5 Conclusion

High energy heavy ion collision is dedicated to research the properties of QGP, in which quarks and gluons behaves as free particle. The most intense magnetic field in the universe is created in it, and the intensity is expected to reach 10^{15} Tesla in LHC energy. Many interesting phenomena such as non-linear QED effects and Chiral Magnetic Effects are expected to be induced under the field. Heavy ion collisions are the only experimental way to generate such an intense field and to study the field-induced phenomena.

Birefringence in vacuum is proposed as a good probe to detect the field because it is only induced by such an intense field. Birefringence induces dilepton polarization which means the decay plane of dilepton from virtual photon can be anisotropic when the virtual photon's momentum is perpendicular to the field. We aim to detect the field with dimuon polarization in ALICE experiment Run 3 planned from 2021 to 2024.

In this study, we evaluated the detectability of Run 3 starting in 2021 to detect strong magnetic field induced muon pair deflection. When muon pairs with fixed decay planes in the actual Run2 data were mixed with 1000 Pb-Pb at a ratio of 1 to calculate the degree of deflection, it was found that Run3 has a sufficiently significant detectability. However, in this study, there are some effects that are ideally assumed, such as the reaction plane resolution, but it is necessary to estimate these detection effects more accurately in consideration of these effects in the future.

References

[1] K. Fukushima and T. Hatsuda, Rep. Prog. Phys. 74 (2011), 014001 The phase diagram of dense QCD

[2] Y.Yamaguchi, "Direct photon measurement with virtual photon method in d+Au collisions at $\sqrt{s_{NN}} = 200$GeV " Tokyo University, doctor thesis(2011)

[3] Annu.Rev.Nucl.Part.Sci.2007.57:205-43

[4] R.Tanizaki, Master Thesis, Hiroshima University

[5] A. Tsuji, Master Thesis, Hiroshima University

[6] K.Tuchin, Phys Rev C 82,034904(2010)

[7] K.Tuchin, Phys Rev C 83,017901(2011)

[8] K.Fukushima, D.E.Kharzeev, H.J.Warringa, Phys.Rev.D 78, 074033(2008)

[9] STAR Collabration, Phys.Rev.C 81,054908(2010), Phys.Rev.Lett 103,251601(2009)

[10] LHC ALICE experiment Japan group `http://alice-j.org/`

[11] cern homepage urlhttp://public.web.cern.ch/public/Welcome.html

[12] `http://aliceinfo.cern.ch/Public/Welcome.html`

[13] Daniel Lohner for the ALICE Collaboration , J. Phys.: Conf. Ser. 446,012028 (2013) Measurement of Direct-Photon Elliptic Flow in Pb-Pb Collisions at $\sqrt{s_{NN}} = 2.76$ TeV

[14] K.Kimura Bachelor Thesis, Hiroshima University

[15] Pythia, Lund University `http://home.thep.lu.se/Pythia/`

[16] Muon Forward Tracker, Letter of Intent `https://cds.cern.ch/record/1592659/files/LHCC-I-022-ADD-1.pdf`

Acknowledgement

I was able to finish my graduation research with the help of many people in the course of this research. First, from the stage of deciding on a theme, my supervisor, Mr. Shigaki, gave me a lot of explanations to myself who did not understand anything, which enabled me to proceed with my research smoothly. I was really grateful to be able to go to talk without shrinking and being very soft. We look forward to your continued support, but we look forward to your continued support. Sugitate-san told me what a researcher should be at the weekly meeting, and I was impressed by how impressed he was. Now I realize that talking to Sugidate-san is all about my growth. I'm really thankful to you. I am very grateful to Professor Homma and Professor Miyoshi for teaching me not only about physics but also about everyday conversations. I was able to do this research with the help of as many seniors as my teachers. In particular, Mr. Yano and Mr. Nagashima taught me various things. I'm very sorry that I was always seeking advice when I was stuck in research. Everyone at the same time, I enjoyed my time in the laboratory every day thanks to you. I felt a bit nervous that it might have hindered my work, but many times I was helped by the kindness of everyone who laughed and went out. Thank you very much. Finally, I want to thank my parents. I was always relieved of the messages that were sent occasionally. I will do my best in the future. I'm really thankful to you.